American Mineralogist, Volume 108, pages 1597–1611, 2023

Apatite in brachinites: Insights into thermal history and halogen evolution

Lang Zhang[1], Ai-Cheng Zhang[1,2,*,†], and Shu-Zhou Wang[1]

[1]State Key Laboratory for Mineral Deposits Research, School of Earth Sciences and Engineering, Nanjing University, Nanjing 210023, China
[2]CAS Center for Excellence in Comparative Planetology, China

Abstract

Apatite is an important petrogenetic indicator in extraterrestrial materials. Here, we report the mineralogical features of apatite and associated phases in three brachinites Northwest Africa (NWA) 4969, NWA 10637, and NWA 11756. Two types of apatite are observed: intergranular apatite and apatite inclusion within chromite and silicate minerals. The intergranular chlorapatite is enclosed by or penetrated by irregular porous merrillite, indicating chlorapatite replacement by merrillite. The intergranular chlorapatite is closely associated with a fine-grained pyroxene-troilite intergrowth along olivine grain boundaries, which is a sulfidization product of olivine. High-Ca pyroxene is observed as a constituent phase in the intergrowth for the first time. The apatite inclusions are either monomineralic or closely associated with subhedral-euhedral pore-free merrillite. In NWA 4969, the apatite inclusions show a large compositional variation from chlorapatite to fluorapatite and are systematically more F-rich than intergranular apatite; while the apatite inclusions in NWA 10637 and NWA 11756 are chlorapatite. Most of the two apatite types in brachinites contain oriented tiny or acicular chromite grains, suggesting the exsolution of chromite from apatite. We propose that apatite replacement by merrillite, formation of pyroxene-troilite intergrowth, and exsolution of chromite in apatite were caused by a shock-induced, transient heating event (~930–1000 °C) on the brachinite parent body. This heating event resulted in halogen devolatilization during replacement of the intergranular apatite by merrillite, which probably disturbed the Mn-Cr isotopic system in brachinites as well. We also propose that the apatite inclusions could be a residual precursor material of the brachinites.

Keywords: Apatite, merrillite, halogen, replacement, sulfidization, exsolution, brachinite; Experimental Halogens in Honor of Jim Webster

Introduction

Apatite [$Ca_5(PO_4)_3(F,Cl,OH)$] is a ubiquitous mineral in most terrestrial and extraterrestrial materials. It is an important carrier of both volatile elements (F, Cl, and OH) and rare earth elements (REE) (Harlov 2015; Hughes and Rakovan 2015). In the past decades, apatite in extraterrestrial materials has been extensively studied to: (1) constrain the petrogenesis and chemical evolution of host rocks (e.g., Shearer et al. 2011; Ward et al. 2017, and references therein); (2) reconstruct the abundance, origin, and evolution of halogen elements and hydrogen on Mars, Moon, and asteroids (e.g., McCubbin and Jones 2015; McCubbin et al. 2015; Ward et al. 2017; Brearley and Jones 2018; McCubbin et al. 2021, and references therein); and (3) determine the age of geological events that its host rocks experienced (e.g., Norman and Nemchin 2014; Yin et al. 2014; Zhang et al. 2016; Zhou et al. 2018; Hu et al. 2019; Li et al. 2021, and references therein).

Brachinites are a group of primitive achondrites that are characterized by the dominance of equigranular FeO-rich olivine (>70 vol%; Krot et al. 2014; Keil 2014; Mittlefehldt 2014). Previous investigations have proposed that brachinites are partial melt residues (e.g., Nehru et al. 1983; Day et al. 2012, 2019; Gardner-Vandy et al. 2013; Keil 2014; Collinet and Grove 2020, and references therein), although some brachinites have been described as cumulates (Warren and Kallemeyn 1989; Swindle et al. 1998; Mittlefehldt et al. 2003). Apatite has occasionally been reported in brachinites or some brachinite-like achondrites; however, its mineralogical features and origins have not yet been studied in detail (e.g., Rumble et al. 2008; Hyde et al. 2014; Keil 2014; Goodrich et al. 2017; Crossley et al. 2020; Ito et al. 2022). All apatite grains reported from brachinites up to date have been chlorapatite (Hyde et al. 2014; Keil 2014; Goodrich et al. 2017; Crossley et al. 2020, and references therein). Hyde et al. (2014) reported that many chlorapatite grains in brachinite Northwest Africa (NWA) 4872 are surrounded by merrillite [$Ca_{18}Na_2Mg_2(PO_4)_{14}$], another common Ca-phosphate mineral in extraterrestrial materials (Jolliff et al. 2006; Shearer et al. 2015). However, the chlorapatite in NWA 4872 was interpreted as an interaction product between merrillite and a Cl-rich melt residuum or low-temperature fluid on the parent body (Hyde et al. 2014).

Previous investigations of brachinites focused mainly on their petrogenesis (e.g., Day et al. 2012, 2019; Keil 2014; Krot et al. 2014; Mittlefehldt 2014, and references therein). In contrast, their post-formation thermal history, which is an important part of the complete evolutionary history in the parent body of brachinites, was less constrained. Two aspects of petrologic records, that could be related to post-formation heating events, have been reported. First, a few brachinites contain pyroxene-troilite intergrowths (e.g., Rumble et al. 2008; Goodrich et al. 2010, 2017;

* E-mail: aczhang@nju.edu.cn. Orcid 0000-0002-5758-0726
† Special collection papers can be found online at http://www.minsocam.org/MSA/AmMin/special-collections.html.

0003-004X/23/0009–1597$05.00/DOI: https://doi.org/10.2138/am-2022-8712

Singerling et al. 2013; Day et al. 2019), whose formation was recently attributed to a reaction between olivine and a S-rich vapor during an impact-induced heating event (Goodrich et al. 2017). Second, Hyde et al. (2014) proposed an alteration event based on the presence of apatite-merrillite intergrowth in brachinite NWA 4872. However, whether the two events are related to each other remains unknown. In addition, a few geochronological investigations on brachinites indicated that the parent body of the brachinites has a rather complex thermal history (Swindle et al. 1998; Wadhwa et al. 1998; Mittlefehldt et al. 2003; Beard et al. 2016; Dunlap et al. 2016a, 2016b). For instance, brachinites have large variations in Mn-Cr and Ar-Ar ages from 4564.8 Ma to ~200 Ma, with some of the ages being attributed to impact events (Dunlap et al. 2016a). However, most of these ages were not discussed in the context of petrologic observations of the brachinites. Recently, Ito et al. (2022) reported young U-Pb ages (<4.5 Ga) of apatite and merrillite in the brachinite NWA 10932 and suggested that an internal heat source rather than impact may be responsible for the formation of phosphate.

To further constrain the thermal history of brachinites, we have performed comprehensive petrographic and mineralogical investigations on three brachinites (NWA 4969, NWA 10637, and NWA 11756). This paper reports the petrography and mineral compositions of apatite and associated minerals in the three brachinites and we then discuss their significance with respect to the thermal history and halogen evolution in the parent body of the brachinites. Preliminary results have been reported in two abstracts in Chinese (Zhang et al. 2021a, 2021b).

Samples and analytical methods

NWA 4969, NWA 10637, and NWA 11756 were classified as brachinites in Meteoritical Bulletin Database (cf. Connolly et al. 2008; Bouvier et al. 2017; Gattacceca et al. 2020). The petrography and mineralogy of NWA 4969 and NWA 11756 have been briefly reported in conference abstracts or journal articles (e.g., Rumble et al. 2008; Gardner-Vandy et al. 2013; Crossley et al. 2020); however, the petrography and mineralogy of NWA 10637 has only been reported in Meteoritical Bulletin Database (Bouvier et al. 2017). The oxygen isotope composition of NWA 10637 ($\Delta^{17}O$ = –0.263 to –0.126 ‰) was also reported in the Database, helping to confirm that NWA 10637 is a brachinite (Bouvier et al. 2017). The three brachinite samples in the present study were purchased from meteorite dealers.

Petrographic observations of the three samples were carried out with the Zeiss Supra 55 field emission scanning electron microscope (FE-SEM) at Nanjing University, Nanjing, China. The FE-SEM instrument was operated at a 15 kV accelerating voltage. Energy dispersive spectroscopic (EDS) point analyses and elemental mapping were also used to qualitatively identify minerals in the regions of interest. Mosaic backscattered electron (BSE) imaging and X-ray elemental mapping for the polished sections were carried out and used for calculating the modal abundances of the constituent minerals.

Mineral compositions were measured using the JEOL 8100 and 8230 electron probe micro-analyzers (EPMA) at Nanjing University. A 20-nA beam accelerated at 15 kV was used for the EPMA analyses of silicate and oxide minerals, while a 10 nA beam accelerated at 10 kV was used for the measurements of merrillite. Olivine, pyroxene, chromite, and merrillite were analyzed with a focused beam; whereas plagioclase was analyzed with a defocused beam (3 μm). For most elements, the counting times for the peak and background measurements were 20 and 10 s, respectively. For Na and K, 10 and 5 s were used for peak and background measurements, respectively. Sodium and K were the first elements measured on their respective spectrometer crystals. Natural fayalite for Fe and Mn; forsterite for Mg; hornblende for Si, Al, Ca, Ti, Na, K; and Durango fluorapatite for P; and synthetic Cr_2O_3 for Cr were used as standards for concentration calibration.

Quantitative measurements of apatite with EPMA are challenging, especially for some apatite grains in this study that have very low F concentrations. We used the LDE1 crystal for determining the F concentration in apatite. Due to the low concentration of F in most apatite grains in the present study, we performed qualitative scanning on Durango apatite standard and some apatite grains in the present study prior to quantitative measurements at various accelerating voltages (10, 12, and 15 kV), beam currents (5, 10, and 20 nA), and focusing modes (focused and 3 μm defocused). Eventually, an accelerating voltage of 15 kV and a defocused 3 μm beam of 20 nA were settled upon for the apatite analyses, since repeatable results could be obtained with this analytical condition for the standards. The elemental peak for F was preset to an L value (the distance between X-ray source and LDE1 analyzing crystal) of 84.15 mm and the lower and upper backgrounds were preset to –6 mm and +17 mm, respectively, based on qualitative scanning results. Chlorine and F were the first elements measured on their respective spectrometer crystals. Durango fluorapatite was used as the standard for P, Ca, and F. A synthetic $Ba_5(PO_4)_3Cl$ crystal was used as the standard for Cl. Standards for other elements are the same as those for the silicate minerals mentioned above. All the EPMA data were reduced using the ZAF correction procedure. Based on multiple analyses on Durango fluorapatite and $Ba_5(PO_4)_3Cl$, the uncertainties for Cl and F are better than 7%. However, the potential anisotropic diffusion effect was not considered in the present study (Henderson 2011 and references therein). Hence, it is possible that the analytical uncertainties for the concentrations of Cl and F might be larger than 7%.

Trace element concentrations in apatite and merrillite were measured using laser ablation inductively coupled plasma mass spectrometry (LA-ICP-MS) at Nanjing University. The target minerals were ablated using a Reso LR155 Excimer 193 nm laser ablation system, connected to ICap Q mass spectrometer. A 4 Hz laser repetition rate was used for the ablation. A 20 μm laser spot size was used for the analyses. The counting times for both background and target phases are 30 s. Durango was used as the external standard; while other four synthetic glasses NIST-610, NIST-612, and NIST-614 were measured as unknowns to monitor data quality. Calcium was used as the internal standard. Trace element abundances were calculated by normalizing the CaO contents in the apatite and merrillite to the values measured by EPMA. Data reduction was performed using the ICPMSDataCal (V9.5) software package (Liu et al. 2008).

Results

General petrography of the three brachinites

Representative mosaic BSE images and elemental mapping results of the three brachinites are shown in Online Materials[1] Figs. S1–S3). All three brachinites show an equigranular texture of silicate minerals (mainly 300–800 μm in grain size). Olivine is the dominant phase but has various modal abundances among different samples (94 vol% in NWA 4969; 73 vol% in NWA 10637; 72 vol% in NWA 11756; Table 1). Pyroxene also has a large variation in modal abundance. In NWA 4969, the intergranular pyroxene is high-Ca pyroxene (2.4 vol%); no intergranular orthopyroxene grains were observed. Both NWA 10637 and NWA 11756 have high abundances of pyroxene (20.7 and 19.8 vol%, respectively). The intergranular pyroxene therein contains both orthopyroxene and high-Ca pyroxene, and orthopyroxene is dominant (Table 1). In these brachinites, chromite, plagioclase, Ca-phosphate minerals, and troilite occur as accessory phases with various abundances (Table 1). A few rounded olivine, pyroxene, and Ca-phosphate inclusions (<100 μm) are also observed (e.g., Online Materials[1] Fig. S4). Fe-oxide/hydroxide, a terrestrial weathering product of Fe-Ni metal and/or sulfide, is widely observed in all three samples. However, the abundance

Table 1. Modal abundances of minerals in three brachinites

	NWA 4969	NWA 10637	NWA 11756
Olivine	94.1	73.2	72.0
High-Ca pyroxene	2.4	3.9	6.6
Orthopyroxene	None	16.8	13.2
Plagioclase	None	0.2	0.1
Chromite	1.0	0.6	0.7
Ca-phosphates	0.1	Trace	0.1
Troilite	0.9	0.1	1.0
Fe-oxide/hydroxide	1.5	5.2	6.3
Total	100	100	100

of Fe-oxide/hydroxide phases in NWA 4969 is much lower than those in NWA 10637 and NWA 11756 (Table 1; Online Materials[1] Figs. S1–S3). An amorphous Fe-phosphate phase, a possible terrestrial weathering product (Hyde et al. 2014), was also observed in NWA 4969 and NWA 11756.

Fine-grained pyroxene-troilite intergrowths, which have been reported in a few other brachinites (e.g., Rumble et al. 2008; Day et al. 2012; Goodrich et al. 2010, 2017), also occur along olivine grain boundaries in all three brachinites in this study (Fig. 1). However, in contrast to previous investigations, our elemental mapping results reveal that the intergrowths contain not only orthopyroxene but also high-Ca pyroxene, although the latter is less abundant (Fig. 1). Some tiny metal grains (<1 μm) also occur in a few intergrowths. It is noteworthy that the pyroxene-troilite intergrowth is common in NWA 4969 and NWA 11756. However, in NWA 10637, only four small regions, (<30 μm in

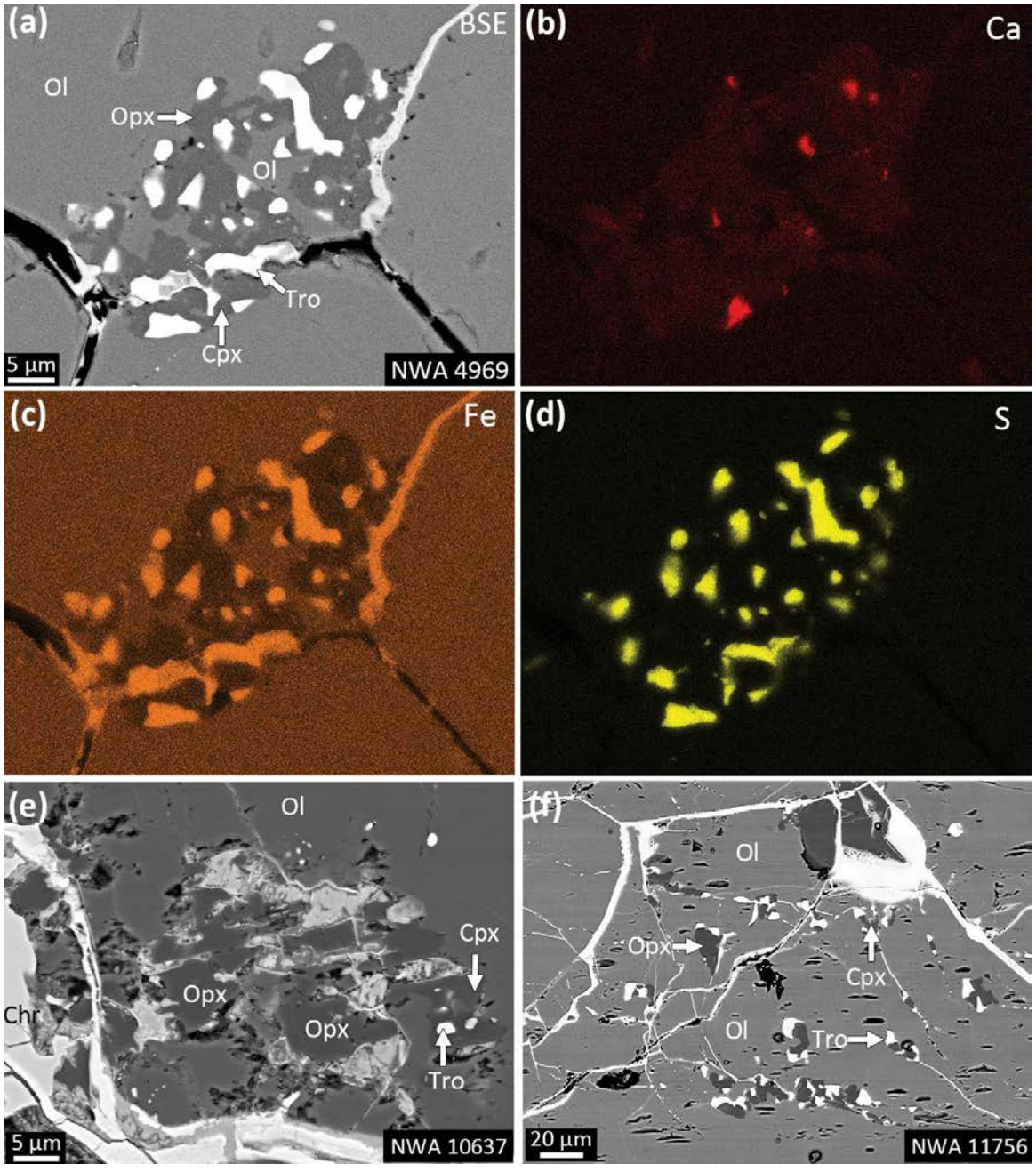

Figure 1. BSE images and SEM-EDS mapping of fine-grained pyroxene-troilite intergrowths in brachinites. (**a**) A typical pyroxene-troilite intergrowth in NWA 4969. (**b**–**d**) maps of Ca, Fe, and S of the region shown in **a**. (**e**) A region in NWA 10637 shows a pyroxene-troilite intergrowth. Troilite in this region has been largely altered during terrestrial weathering. (**f**) A region in NWA 11756 shows fine-grained pyroxene-troilite intergrowths. Ol = olivine; Opx = orthopyroxene; Cpx = high-Ca pyroxene; Tro = troilite; Chr = chromite. (Color online.)

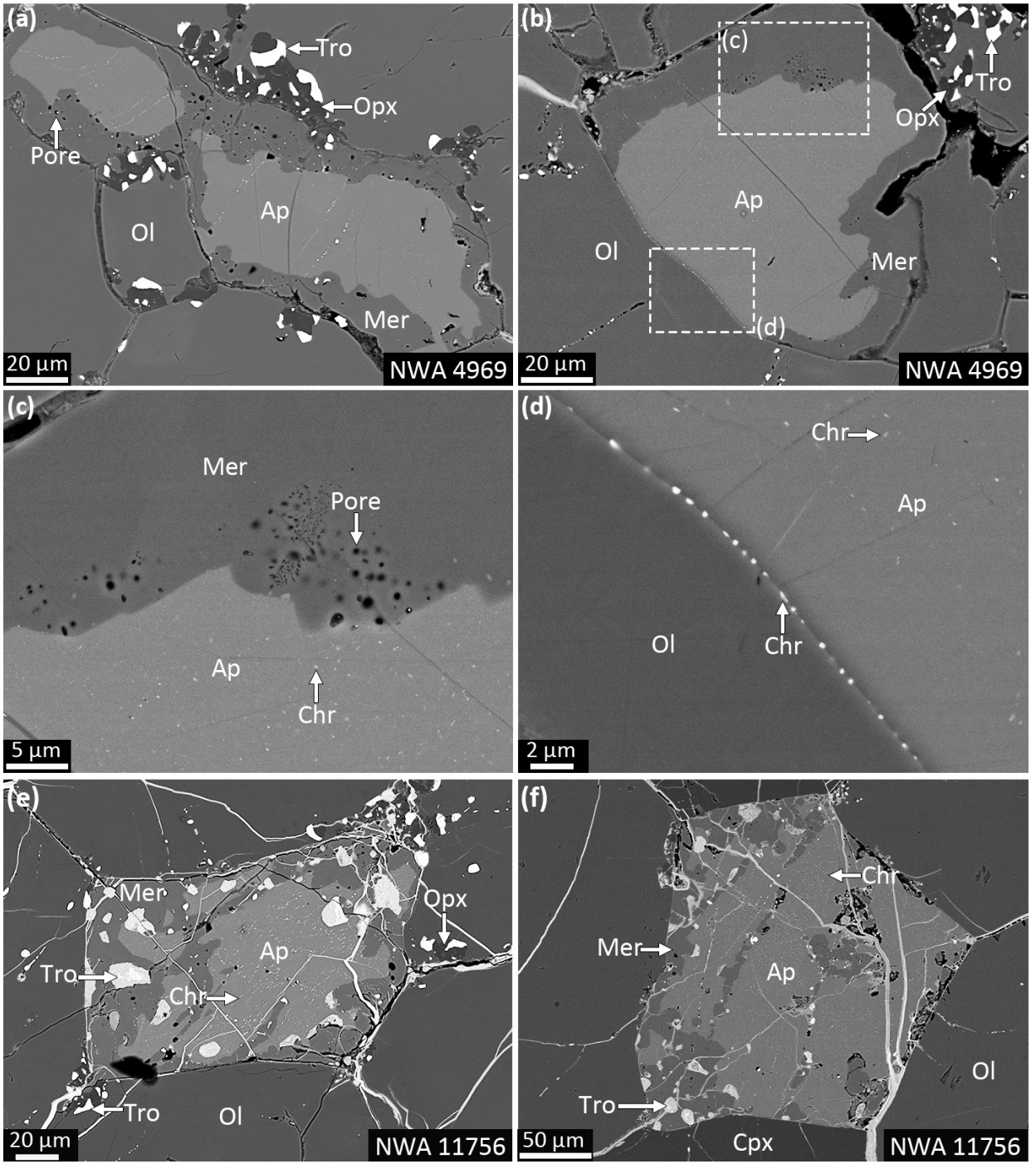

Figure 2. BSE images of intergranular apatite in brachinites. (**a**–**b**) Relatively coarse, irregularly shaped apatite grains are rimmed with merrillite. Tiny pores are present in merrillite grains. Note that pyroxene-troilite intergrowths are closely associated with the apatite-merrillite assemblage. (**c**) Higher magnification image of the upper rectangle outlined in **b** showing the pores in merrillite adjacent to the interface with apatite. Many tiny chromite grains are present in the apatite grain interior. (**d**) Higher magnification image of the other rectangle outlined in **b** showing the chromite grains at the boundary between apatite and olivine. (**e**–**f**) Intergranular apatite and merrillite in NWA 11756. The apatite grains have been partially replaced by irregular merrillite. The apatite grains contain tiny acicular chromite grains. Fine-grained pyroxene-troilite intergrowths are also present adjacent to the intergranular apatite (**e**). Ol = olivine; Ap = apatite; Mer = merrillite; Chr = chromite; Cpx = high-Ca pyroxene; Opx = orthopyroxene; Tro = troilite.

the largest dimension), containing a potential pyroxene-troilite intergrowth, were observed. Here high-Ca pyroxene is very rare (only 3 submicrometer high-Ca pyroxene grains in three of the four regions).

Mineralogy of apatite and associated merrillite

Apatite has two different occurrences in the three brachinites. One is as intergranular apatite between silicate minerals and is always associated with merrillite (Fig. 2). The other is as rounded apatite included within chromite or silicate minerals (Figs. 3 and 4). Both types of apatite are present in NWA 4969 and NWA 11756; however, in NWA 10637, apatite occurs only as a mineral inclusion.

In NWA 4969, intergranular apatite is commonly surrounded by merrillite (Figs. 2a and 2b). The outlines of the apatite-merrillite assemblage conform to the shapes of the surrounding equigranular silicate grains. The grain boundaries between apatite and merrillite are irregularly shaped (Figs. 2a and 2b). Many intergranular merrillite grains in NWA 4969 contain submicrometer-sized pores adjacent to the boundary with apatite (Figs. 2a and 2c). The intergranular apatite-merrillite assemblage is spatially associated with pyroxene-troilite intergrowths (Figs. 2a and 2b). In the polished sections made from NWA 4969, about 50 apatite inclusions were observed. Most of them are included in chromite and monomineralic. A few apatite inclusions themselves contain subhedral-euhedral, pore-free merrillite grains at their margins,

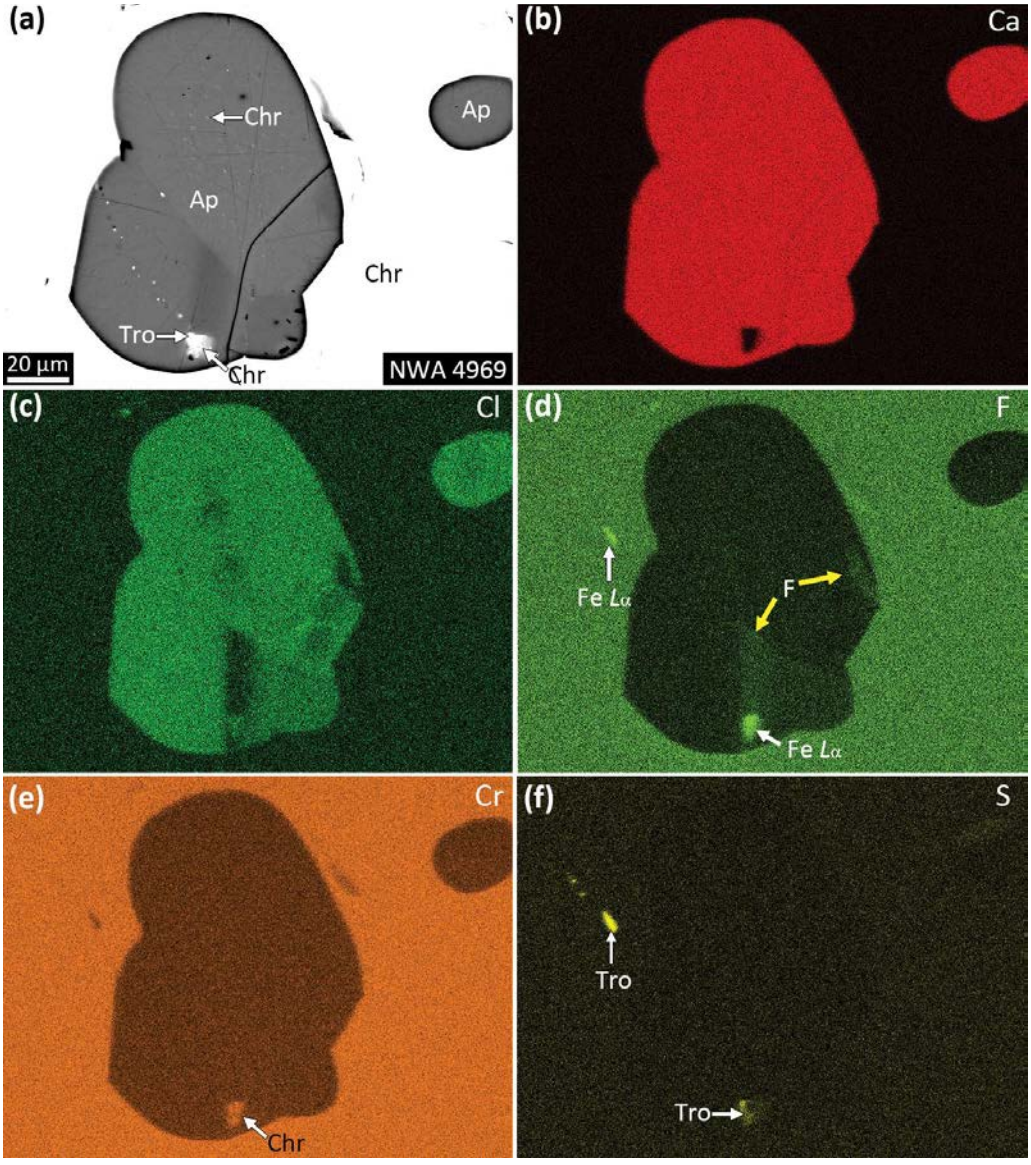

Figure 3. BSE image (**a**) and SEM-EDS mapping (**b**–**f**) of apatite inclusions within an intergranular chromite grain in NWA 4969. (**a**) The central part of this image shows at least three grains with a Z-contrast variation in the BSE image of apatite inclusions in chromite. (**c**) The Cl map shows that the dark regions in **a** are relatively Cl poor. (**d**) The F-rich apatite grains are indicated by yellow arrows. However, the two hot spots and the region surrounding the F-poor apatite grains in **d** show the signals from Fe*Lα* rather than F*Kα*. (**e**–**f**) Results from Cr and S mapping. Chr = chromite; Ap = apatite; Tro = troilite. (Color online.)

which is different from the texture of the intergranular apatite and merrillite. An apatite aggregate of approximately 40 μm in size included within one chromite grain shows a marked Z-contrast variation in the BSE image (Fig. 3a). Elemental mapping results demonstrate that the Z-contrast variation among and within the apatite grains is related to variations in the Cl and F contents (Figs. 3c and 3d). High-magnification SEM observations show that both the intergranular apatite and the apatite inclusions usually contain oriented tiny or acicular chromite inclusions (Fig. 2c). In addition, tiny chromite grains (submicrometer in size) also occur at the grain boundaries between the apatite and adjacent olivine (Fig. 2d).

In NWA 11756, the intergranular chlorapatite-merrillite assemblage also has outlines conforming to the shapes of the surrounding silicate grains (Figs. 2e and 2f). However, the texture of the chlorapatite-merrillite assemblage differs slightly from that in NWA 4969. First, the merrillite/chlorapatite volume ratio in NWA 11756 appears to be lower than that in NWA 4969. Second, merrillite in NWA 11756 mainly appears as irregular grains along fractures in the chlorapatite and along the interface with the surrounding silicate phases. Small pores also occur in a few intergranular merrillite grains in NWA 11756, although less common than in NWA 4969. The intergranular apatite-merrillite assemblage in NWA 11756 is also spatially associated with a pyroxene-troilite intergrowth (Fig. 2e). The apatite inclusions (5–100 μm) in NWA 11756 mainly occur within olivine and orthopyroxene. In one case, the olivine grain containing a subhedral-euhedral apatite grain is itself included within a coarse chromite grain (Fig. 4a). Most apatite inclusions in NWA 11756 are also closely associated with merrillite. Differing from the intergranular merrillite, most of the merrillite grains associated with the apatite inclusions are subhedral to euhedral in shape and included by the latter (Fig. 4b). They are pore-free and sometimes contain tiny sulfide grains. Similar to apatite in NWA 4969, the intergranular apatite grains and the apatite grains in NWA 11756 also contain tiny chromite grains in the grain interiors and some of the chromite grains are acicular (Figs. 2e and 2f). Some tiny chromite grains also occur at the grain boundaries between the apatite inclusions and the host silicate minerals (Fig. 4b).

In NWA 10637, the apatite grains are present only as inclusions (Figs. 4c and 4d). No intergranular apatite grains were observed in this study. The apatite inclusions usually form

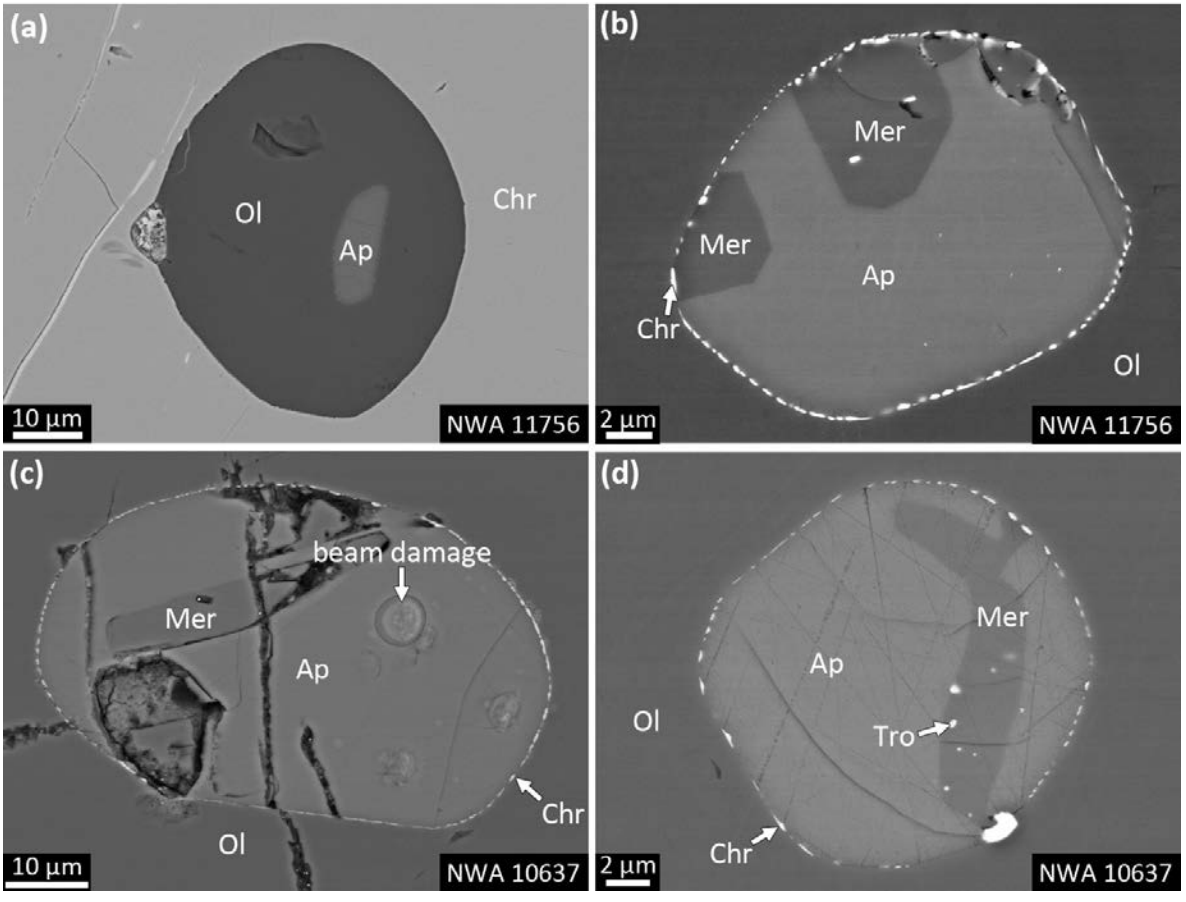

Figure 4. BSE images of apatite inclusions in NWA 11756 and NWA 10637. (**a**) A euhedral apatite grain is included in an olivine grain, which itself is included in chromite from NWA 11756. (**b**) A rounded apatite inclusion within olivine from NWA 11756. Several euhedral merrillite grains occur at the margin of the apatite inclusion. Tiny chromite grains are also present at the boundary between the apatite and olivine. (**c**–**d**) Subhedral-euhedral merrillite grains are included in the rounded apatite inclusions within olivine from NWA 10637. Note that many tiny chromite grains occur at the boundary between apatite and olivine. Ap = apatite; Mer = merrillite; Chr = chromite; Ol = olivine; Tro = troilite.

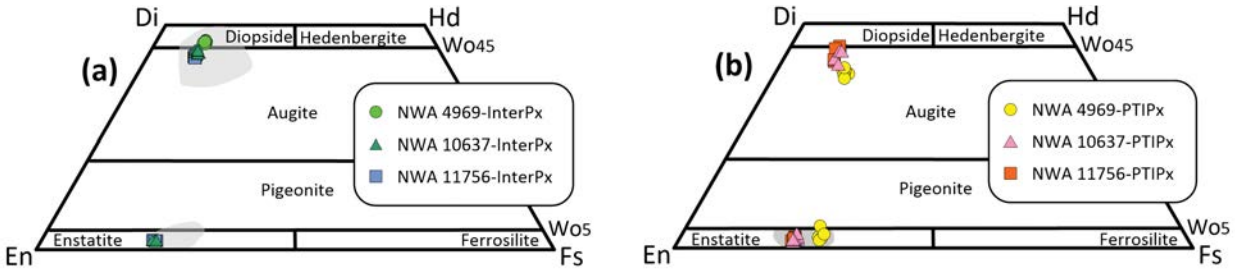

Figure 5. Quadrilateral diagrams showing the major-element compositions for intergranular pyroxenes (**a**) and pyroxenes in pyroxene-troilite intergrowths (**b**) from the brachinites in this study. InterPx = intergranular pyroxene; PTIPx = pyroxene in pyroxene-troilite intergrowth. The gray regions show the compositional ranges of pyroxenes reported in literature (Nehru et al. 1983; Warren and Kallemeyn 1989; Swindle et al. 1998; Mittlefehldt et al. 2003; Goodrich et al. 2006, 2010; Rumble et al. 2008; Gardner-Vandy et al. 2013; Day et al. 2015, 2019; Crossley et al. 2020). (Color online.)

intergrowths (10–30 μm) with subhedral-euhedral merrillite. In some cases, euhedral merrillite grains are totally included in apatite (Fig. 4c). Tiny chromite grains (<1 μm) are commonly observed at the boundaries between included apatite and the host olivine (Figs. 4c and 4d).

Major- and minor-element compositions of minerals

EPMA compositions of the major and minor elements in minerals from the three brachinites (olivine, pyroxene, plagioclase, chromite, and Ca-phosphates) are reported in the Online Materials[1] Tables S1 through S7.

All olivine grains in the three brachinites are FeO rich. The Fo values [≡100·Mg/(Mg+Fe)] of equigranular olivine in NWA 4969, NWA 10637, and NWA 11756 are 65.4–66.4, 72.7–73.7, and 72.7–73.8, respectively. The olivine inclusions in NWA 4969 are more magnesian ($Fo_{66.7–68.2}$) than the equigranular olivine in the same sample; while the compositions of the olivine inclusions in NWA 10637 and NWA 11756 are comparable to those of the intergranular olivine grains in the same samples (Online Materials[1] Table S1).

Major-element and minor-element compositions of pyroxenes in the three brachinites are illustrated in Figs. 5–7. The intergranular high-Ca pyroxene in NWA 4969 contains slightly higher Wo components than those in NWA 10637 and NWA 11756 (Online Materials[1] Table S2; Fig. 5a). The Al_2O_3, TiO_2, and Cr_2O_3 contents are comparable among the intergranular high-Ca pyroxene in the three brachinites (Fig. 6). Intergranular orthopyroxene grains in NWA 10637 and NWA 11756 have essentially identical major-element compositions (Online Materials[1] Table S2; Fig. 5). They have similar TiO_2 and Cr_2O_3

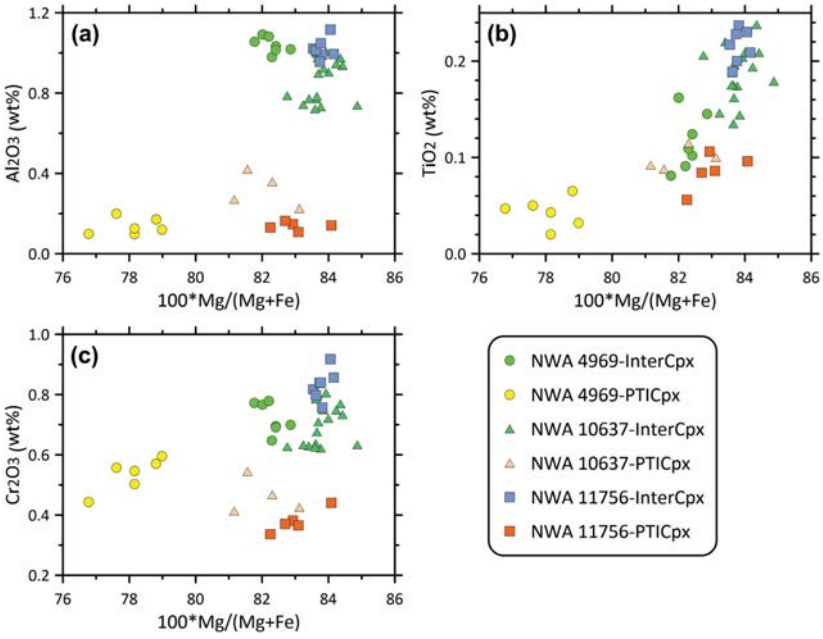

Figure 6. Al_2O_3 (**a**), TiO_2 (**b**), and Cr_2O_3 (**c**) vs. the Mg/(Mg+Fe) molar ratio in high-Ca pyroxene from the brachinites in this study. The high-Ca pyroxene in the pyroxene-troilite intergrowths shows systematically lower contents of Al_2O_3, TiO_2, and Cr_2O_3 than the intergranular high-Ca pyroxene in the same meteorites, respectively. InterCpx = intergranular high-Ca pyroxene; PTICpx = high-Ca pyroxene in the pyroxene-troilite intergrowth. (Color online.)

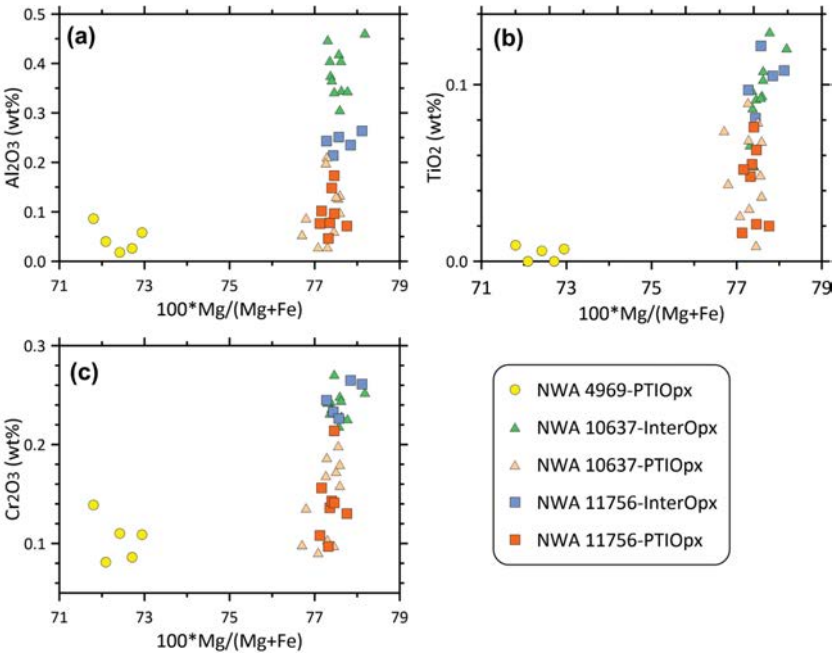

Figure 7. Al_2O_3 (**a**), TiO_2 (**b**), and Cr_2O_3 (**c**) vs. the Mg/(Mg+Fe) molar ration in orthopyroxene from the brachinites in this study. The orthopyroxene in the pyroxene-troilite intergrowths shows systematically lower contents of Al_2O_3, TiO_2, and Cr_2O_3 than the intergranular orthopyroxene (if present) in the same meteorites. PTIOpx = orthopyroxene in pyroxene-troilite intergrowth; InterOpx = intergranular orthopyroxene. (Color online.)

contents and slightly different Al_2O_3 contents (Online Materials[1] Table S2; Fig. 7). Based on the two-pyroxene thermometer in Brey and Köhler (1990), paired high-Ca pyroxene and orthopyroxene give an equilibrium temperature of 929 ± 21 °C and 972 ± 10 °C for NWA 10637 and NWA 11756, respectively. Compositions of the orthopyroxene inclusions within chromite from NWA 10637 and NWA 11756 were also measured. However, the data show anomalously high-Cr_2O_3 contents (1.4–1.7 wt%), which could be due to potential analytical contamination from the host chromite. Therefore, the data are not reported here.

Fine-grained high-Ca pyroxene and orthopyroxene in the pyroxene-troilite intergrowths from NWA 10637 have major-element compositions essentially identical to those from NWA 11756 (Online Materials[1] Table S3; Fig. 5). However, high-Ca pyroxene and orthopyroxene in the intergrowths from NWA 4969 have major-element compositions different from those in NWA 10637 and NWA 11756 (Online Materials[1] Table S3; Fig. 5). The high-Ca pyroxene and orthopyroxene in the intergrowths show systematically lower contents of Al_2O_3, TiO_2, and Cr_2O_3 than those in the intergranular pyroxenes from the same samples (Online Materials[1] Table S3; Figs. 6 and 7). Based on the two-pyroxene thermometer in Brey and Köhler (1990), the paired high-Ca pyroxene and orthopyroxene in the intergrowths give equilibrium temperatures of 1015 ± 16 °C, 932 ± 63 °C, and 938 ± 51 °C for NWA 4969, NWA 10637, and NWA 11756, respectively.

Plagioclase grains in both NWA 10637 and NWA 11756 are mainly sodic and have similar An values (An = 34.6–35.4 and 33.1–35.1, respectively; Online Materials[1] Table S4). Only the coarse chromite grains in the three brachinites were measured. The chromite grains in NWA 10637 and NWA 11756 have essentially identical compositions. They have higher Cr# [≡100·Cr/(Al+Cr)] values (77.1–77.7) than those in NWA 4969 (73.0–73.5; Online Materials[1] Table S5). Their TiO_2 contents (1.0–1.1 wt%) are also higher than those in chromite from NWA 4969 (0.56–0.64 wt%).

The F-Cl compositions from apatite are plotted in a ternary diagram for F, Cl, and the missing component, likely OH (Fig. 8). The amounts of the missing component are assumed to be 1-F-Cl. The present study mainly focuses on the fluorapatite and chlorapatite components. The intergranular apatite grains in NWA 4969 are chlorapatite with a 10 to 16 mol% fluorapatite component (Online Materials[1] Table S6; Fig. 8a). Most of the apatite inclusions in NWA 4969 are also chlorapatite, but contain a fluorapatite component comparable to or higher than those of the intergranular grains (Online Materials[1] Table S6; Fig. 8a). A few apatite inclusions (Fig. 3) are fluorapatite with fluorapatite component as high as 78 mol%. The fluorapatite grains contain much lower Na_2O (<0.06 wt%) than the chlorapatite (0.3–0.6 wt%). The apatite inclusions in NWA 10637 are also chlorapatite, with the fluorapatite component varying from 0 to 13 mol% (Fig. 8b). The intergranular apatite grains and the apatite inclusions in NWA 11756 have comparable compositions with the fluorapatite component varying from 4 to 18 mol% (Fig. 8c). The chlorapatite in NWA 10637 and NWA 11756 contains a similar Na_2O content (0.3–0.5 wt%).

The merrillite grains in this study have similar MgO contents (Online Materials[1] Table S7). There are small variations in FeO and Na_2O between different samples or between different occurrences (Online Materials[1] Table S7). The merrillite grains associated with intergranular apatite and apatite inclusions in NWA 4969 have similar FeO (0.83–1.21 wt% and 0.88–1.28 wt%, respectively) and Na_2O (2.62–2.96 wt% and 2.68–2.92 wt%,

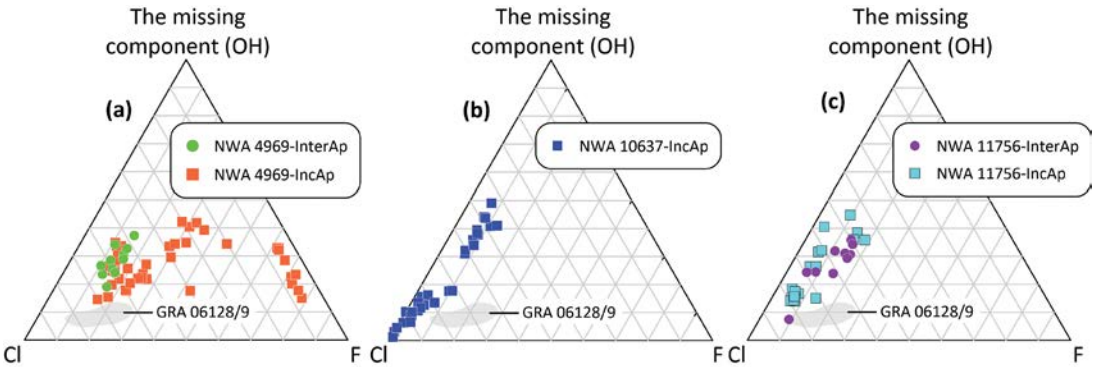

Figure 8. Ternary plot of apatite halogen compositions in NWA 4969 (**a**), NWA 10637 (**b**), and NWA 11756 (**c**), compared with apatite from GRA 06128/9 (McCubbin and Jones 2015). The amounts of the missing component are assumed to be 1-F-Cl. InterAp = intergranular apatite; IncAp = apatite inclusion within chromite or silicate minerals. (Color online.)

respectively) contents. The FeO contents in the intergranular merrillite from NWA 11756 (0.52–1.02 wt%) are comparable to those in NWA 4969. However, the merrillite inclusions in NWA 10637 and NWA 11756 have FeO contents (1.15–1.45 wt% and 1.35–1.64 wt%) slightly higher than those in NWA 4969. The merrillite grains associated with intergranular apatite and apatite inclusions in NWA 10637 and NWA 11756 show similar Na_2O contents (1.75–2.64 wt%), which are slightly lower than those in NWA 4969.

Trace-element concentrations of intergranular apatite and merrillite

In total, 21 trace-element point analyses were carried out on intergranular apatite and associated merrillite. The data are given in Online Materials[1] Table S8 and illustrated in Figures 9 and 10. Both intergranular apatite and merrillite in NWA 4969 exhibit a generally flat REE pattern with a small positive Eu anomaly [Eu/Eu* = 1.3–3.8, where $Eu/Eu^* \equiv Eu_N/\sqrt{(Sm_N \cdot Gd_N)}$; Fig. 9a]. The REE concentrations in merrillite (La = 17.5–22.2·CI) from NWA 4969 are approximately two times higher than those of chlorapatite (La = 6.6–10.4·CI; Online Materials[1] Table S8). The apatite and merrillite in NWA 11756 also show flat REE patterns with a small positive Eu anomaly (1.6–11.6; Fig. 9b). However, the merrillite REE concentration (La = 16.6·CI) is much higher than that of apatite (1.0–3.7·CI; Online Materials[1] Table S8; Fig. 9b).

Both the apatite and merrillite grains in this study have low concentrations of Th (0.15–0.34 ppm and 0.18–0.37 ppm, respectively) and U (0.02–0.15 ppm and 0.02–0.19 ppm, respectively; Fig. 10). No sample- or mineral-dependent variations were observed.

Discussion

Replacement of intergranular apatite by merrillite

In extraterrestrial materials, apatite and merrillite show various textural relationships (e.g., Zhang et al. 2010; Shearer et al. 2011; Day et al. 2012; Sarafian et al. 2013; Hyde et al. 2014; Jones et al. 2014, 2016; Howarth et al. 2015; McCubbin and Jones 2015; Zhang et al. 2016; Ward et al. 2017). Apatite and merrillite in lunar and Martian basalts usually occur either as subhedral-euhedral individual grains or show an intergrowth texture (e.g., Zhang et al. 2010; Howarth et al. 2015; McCubbin and Jones 2015). In lunar samples, this feature was interpreted to be a co-crystallization from basaltic melts (e.g., Zhang et al. 2010). However, their coexistence in Martian basalts was interpreted as a reaction product between merrillite and a Cl-

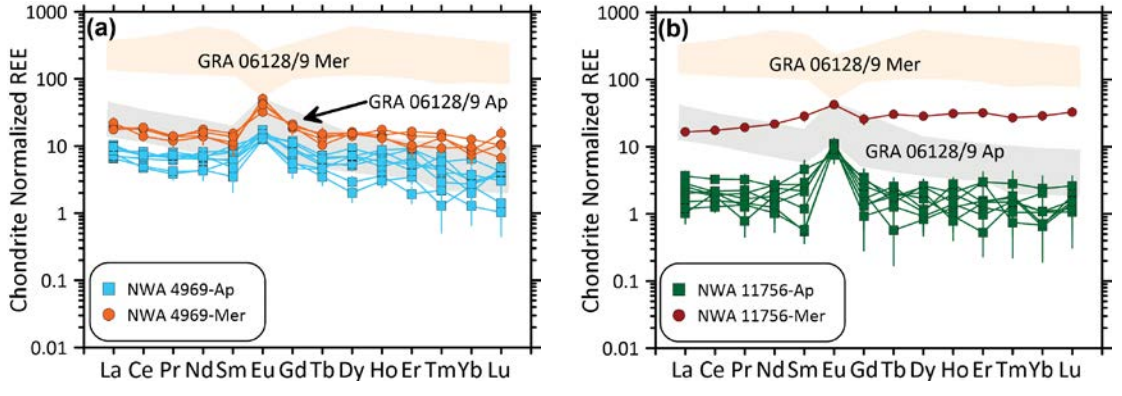

Figure 9. Chondrite-normalized REE patterns of intergranular Ca-phosphate minerals in in NWA 4969 (**a**) and NWA 11756 (**b**). The shaded regions show the REE patterns of apatite and merrillite from GRA 06128/9 (Shearer et al. 2010; Day et al. 2012; Zhou et al. 2018). The reference data for the CI chondrite is adopted from Barrat et al. (2012). The error bar is 1σ. (Color online.)

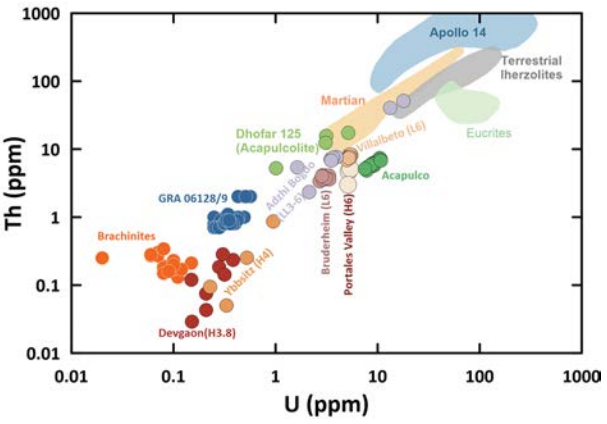

Figure 10. U-Th compositions of apatite in brachinites and comparison with those in other extraterrestrial materials. The composition data of brachinites are from this study. The composition data for apatite in GRA 06128/9 are from Zhou et al. (2018). Other composition data and regions are from Ward et al. (2017) and references therein. (Color online.)

rich hydrothermal fluid (e.g., Howarth et al. 2015; McCubbin and Jones 2015; McCubbin et al. 2016). Jones et al. (2014) and McCubbin and Jones (2015) proposed that the chlorapatite in chondritic meteorites formed through reactions between merrillite and metasomatic fluids. A similar interpretation has also been applied to the complex textural relationship between chlorapatite and merrillite in the GRA 06128/9 achondrites (Shearer et al. 2011), although intergrowth was also proposed as an alternative (e.g., Day et al. 2012). Hyde et al. (2014) reported that merrillite is present along the edges of some of the chlorapatite grains in the NWA 4872 brachinite. However, they proposed that the merrillite is magmatic in origin and that the chlorapatite formed from a reaction between merrillite and a Cl-rich melt residuum or lower-temperature fluids on the parent body (Hyde et al. 2014).

In NWA 4969 and NWA 11756, merrillite always occurs along the edges of the intergranular apatite grains or penetrates the interior of the apatite grains, similar to the texture of intergranular Ca-phosphate minerals in NWA 4872 (Hyde et al. 2014). Particularly, in NWA 4969, many intergranular apatite grains are partly or completely enclosed by porous merrillite. Although such a texture is consistent with a replacement origin, it is contrary with the interpretation that apatite formed by reaction between merrillite and Cl-rich fluids (Hyde et al. 2014). In typical replacement textures, secondary mineral or mineral assemblage usually encloses the relict primary mineral or penetrates into the fractures in primary mineral (e.g., Putnis 2002, 2009; Altree-Williams et al. 2015; Harlov 2015). Therefore, it is more likely that the intergranular apatite grains were partly replaced by merrillite along the interface with the surrounding silicate minerals or fractures in the original apatite grains. In NWA 4969, small pores in merrillite occur only in regions adjacent to the interface with apatite. The apatite grains are themselves free of pores. Such textures also support the interpretation that apatite was replaced by merrillite, since porous textures always develop in the reaction products that form through coupled dissolution-reprecipitation in natural and experimental replaced samples (e.g., Putnis 2002, 2009; Altree-Williams et al. 2015; Harlov 2015). The formation of small pores could be related to volume change and/or mass transfer during replacement (Putnis 2002; Putnis and John 2010). Since the replacement of chlorapatite by merrillite is a devolatilization reaction, Cl-rich fluids, most likely as vapors, were probably lost along the grain boundaries or via the porosity. In addition, the similar REE patterns between intergranular apatite and associated merrillite and the small difference in their concentration in NWA 4969 also support the interpretation that the intergranular apatite was replaced by merrillite.

To our knowledge, no experiments studying the transformation from chlorapatite to merrillite have been reported yet. However, previous investigations involving synthesis and thermal stability of hydroxyapatite and chlorapatite can provide some insights into the replacement of apatite by merrillite in the present study. For instance, Demnati et al. (2012) found that pure chlorapatite powder has a good thermal stability over a large temperature range (30–1400 °C). This result is consistent with the experiments by Adolfsson and Hermansson (2000) that no phase changes were detected in the hot isostatically pressed Al_2O_3-apatite composites. However, Adolfssonn and Hermansson (2000) found that chlorapatite may first react with the moisture in the air and partly convert to oxyhydroxyapatite and then react with Al_2O_3 to form $Ca_3(PO_4)_2$ and $CaAl_2O_4$, if the Al_2O_3-apatite composites were crushed and heat-treated in air. Jang et al. (2015) reported that the presence of Mg^{2+} ions in relatively low-pH solutions may facilitate the transformation from hydroxyapatite to whitlockite, an isomorphous mineral of merrillite, consistent with the observations in Hughes et al. (2008). These experimental results indicate that some minor contaminants in open systems may decrease the thermal stability of chlorapatite and facilitate the formation of whitlockite/merrillite (Hughes et al. 2008). As discussed in the following section, formation of pyroxene-troilite intergrowths in brachinites involves the sulfidization of olivine (Goodrich et al. 2017), which releases minor Mg and Fe. Since the apatite-merrillite assemblage is spatially associated with the pyroxene-troilite intergrowth, it is likely that the release of Mg and Fe during sulfidization of olivine facilitates the replacement of chlorapatite by merrillite.

We note that Hughes et al. (2008) and Jang et al. (2015) obtained whitlockite in solutions at 240 and 70 °C, respectively. If the replacement of apatite by merrillite in brachinites also occurred in solutions at similar temperatures, alteration of olivine to serpentine would be expected to be present. However, no serpentine was observed in either the present study or in previous investigations (e.g., Hyde et al. 2014). This implies that the replacement of apatite by merrillite should take place without aqueous solutions, probably at high temperatures, which is consistent with the high temperatures required for the sulfidization of olivine.

Sulfidization of olivine in brachinites

Pyroxene-troilite intergrowths have been observed in many brachinites (e.g., Rumble et al. 2008; Goodrich et al. 2010, 2017; Singerling et al. 2013; Day et al. 2019). They were interpreted to have resulted from the sulfidization of olivine based on the intergrowth texture (Singerling et al. 2013; Goodrich et al. 2017): $2(Fe,Mg)_2SiO_4 + S_2(g) \leftrightarrow 2MgSiO_3 + 2FeS + O_2(g)$. The same mechanism was also proposed to account for the replacement of

olivine by orthopyroxene and troilite in the Apollo lunar samples (Colson 1992; Norman et al. 1995; Shearer et al. 2012), HED meteorites (Zhang et al. 2018, 2020), and in the ungrouped achondrite Divnoe (Petaev et al. 1994). However, as Goodrich et al. (2017) pointed out, the above reaction equation is too simplistic. If considering the specific compositions of relict olivine and the orthopyroxene in the intergrowths, Si would be somehow gained or Mg and Fe would be released from the system (cf. Shearer et al. 2012; Zhang et al. 2018). In addition, the presence of troilite in the intergrowths indicates that the S fugacity should be buffered by the reaction $FeS \leftrightarrow Fe + ½S_2$ (Shearer et al. 2012; Zhang et al. 2018). This reaction can also account for the presence of minor amounts of Fe-metal in the intergrowths (Shearer et al. 2012; Zhang et al. 2018, 2020).

In the present study, the three brachinites contain pyroxene-troilite intergrowths in various abundances along olivine grain boundaries. Their textures resemble those described in other brachinites (Rumble et al. 2008; Goodrich et al. 2010, 2017; Day et al. 2019). In NWA 10637 and NWA 11756, the small orthopyroxene grains in the intergrowths contain Al_2O_3, TiO_2, and Cr_2O_3, which are systematically lower than those in intergranular orthopyroxene (Fig. 7). Although NWA 4969 contains no intergranular orthopyroxene, the orthopyroxene grains in the intergrowths contain similarly low Al_2O_3, TiO_2, and Cr_2O_3 contents compared to those in NWA 10637 and NWA 11756 (Fig. 7). This Al-Ti-Cr-poor feature of orthopyroxene has also been reported for orthopyroxene in the intergrowths from Divnoe, Apollo lunar samples, and HED meteorites, as an important indicator for the sulfidization origin of pyroxene-troilite intergrowths (Petaev et al. 1994; Shearer et al. 2012; Zhang et al. 2018, 2020). Therefore, the relatively Al,Ti,Cr-poor feature in the present study supports the idea that the pyroxene-troilite intergrowths in brachinites are sulfidization products of olivine (Goodrich et al. 2017).

One of the important observations in the present study is that the pyroxene-troilite intergrowths in brachinites contain not only orthopyroxene but also high-Ca pyroxene, although high-Ca pyroxene is much less abundant than orthopyroxene. The fine high-Ca pyroxene grains in the pyroxene-troilite intergrowths also have Al_2O_3, Cr_2O_3, and TiO_2 contents systematically lower than the intergranular high-Ca pyroxene (Fig. 6). Al,Ti,Cr-poor high-Ca pyroxene was not observed in the pyroxene-troilite intergrowths described in the Divnoe, Apollo lunar samples, and HED meteorites (e.g., Petaev et al. 1994; Shearer et al. 2012; Zhang et al. 2018, 2020). They were also not reported in previous investigations on brachinites, probably due to their low-modal abundance and the difficulty of distinguishing them from the dominant orthopyroxene under BSE imaging. The low contents of Al_2O_3, Cr_2O_3, and TiO_2, compared with intergranular high-Ca pyroxene, imply that the fine-grained high-Ca pyroxene in the intergrowths should be a byproduct during sulfidization of the olivine. Since olivine in brachinites is a Ca-poor phase, the presence of minor high-Ca pyroxene in the intergrowths indicates the addition of external Ca to the system. Because the transformation from apatite (Ca/P ~ 1.67) to merrillite (Ca/P ~ 1.29) releases Ca, this would suggest that the apatite-merrillite transformation supplies the necessary Ca for the formation of Al-Ti-Cr-poor high-Ca pyroxene in the pyroxene-troilite intergrowth. The addition of Ca could also account for the similarity between the Wo components in the intergranular orthopyroxene and the fine-grained orthopyroxene in the intergrowth. For comparison, the fine-grained orthopyroxene in the intergrowth from diogenites and the Apollo lunar samples contains a lower Wo component than those crystallized from mafic to ultramafic magmas (Shearer et al. 2012; Zhang et al. 2018, 2020). If this is correct, the apatite-merrillite transformation and the sulfidization of olivine in brachinites could be coupled during a common heating event. The release of Mg and Fe during sulfidization of olivine facilitates the apatite-merrillite transformation; meanwhile, the release of Ca during apatite-merrillite transformation results in the formation of high-Ca pyroxene in the pyroxene-troilite intergrowth. The presence of orthopyroxene + high-Ca pyroxene assemblage instead of pigeonite is probably due to the instability of pigeonite in the presence of a S-rich vapor (Kullerud and Yoder 1963; Zhang et al. 2013; Wang et al. 2019). Based on temperatures estimated from the paired orthopyroxene and high-Ca pyroxene in the intergrowths, the heating event probably took place at around 930 to 1000 °C, which is consistent with the high temperatures required for sulfidization of silicate minerals (Kullerud and Yoder 1963).

In brachinites, the pyroxene-troilite intergrowths are present only along olivine grain boundaries (Rumble et al. 2008; Singerling et al. 2013; Goodrich et al. 2017; this study). This textural feature indicates that the S-rich material reacting with olivine must have been able to permeate the rock along the olivine grain boundaries. The most likely phase that could cause these features is a S-rich vapor. In the previous investigations that studied sulfidization of olivine and pyroxene, two potential mechanisms have been proposed to account for the generation of S-rich vapors: (1) degassing during magma emplacement may generate S-rich vapors (Shearer et al. 2012), and (2) impact events may remobilize S in projectile or target materials (Zhang et al. 2013; Goodrich et al. 2017; Wang et al. 2019). Goodrich et al. (2017) argued that generation of S-rich vapors in the parent bodies of brachinites and brachinite-like achondrites cannot be explained by magma degassing during magma emplacement, considering the difficulty of generating multiple melting events on a primitive achondrite parent body. Therefore, they suggested that the S-rich vapors would be generated elsewhere by impact events and migrate into the brachinites and brachinite-like achondrites (Goodrich et al. 2017). In the present study, we concur that impact-induced formation mechanism was the most likely source of S-rich vapors. However, the observations in this study cannot totally exclude the possibility that impact-induced S-rich vapor had a local source since brachinites themselves contain sulfide grains. This takes into account that S is readily remobilized along heated grain boundaries during shock metamorphism (Sharp and DeCarli 2006).

Exsolution of chromite in apatite

The present study shows that almost all the apatite grains in the three brachinites contain oriented tiny or acicular chromite grains. To our knowledge, this is the first description about acicular chromite inclusions within apatite. Harlov (2015) reported monazite and/or xenotime inclusions in reacted apatite grains, with the unreacted apatite grains themselves containing no such inclusions. They proposed that the inclusions formed via coupled dissolution-reprecipitation with fluids (Harlov 2015). However, this scenario cannot account for the presence

of acicular chromite inclusions in both the relict intergranular apatite grains and the apatite inclusions within chromite (Figs. 2 and 3). Instead, the textural correlation between tiny chromite grains and host/surrounding apatite grains resembles the occurrences of subparallel acicular chromite within Fe-rich olivine and of chromite surrounding olivine in weakly metamorphosed ordinary chondrites (L3.1/3.2), which was proposed to be an exsolution product of chromite from olivine (Grossman and Brearley 2005). Based on the textural similarity, we suggest that the parallel acicular chromite grains could be an exsolution product from originally Cr-bearing chlorapatite. However, no phase diagram exists showing the relationship between chromite and apatite, although Cr^{3+} is expected to be present in the apatite structure (Maunaye et al. 1976; Pan and Fleet 2002; Hughes and Rakovan 2015). There is no information on diffusion rates of Cr and Fe in apatite in the literature. Therefore, it is difficult to directly constrain the exsolution temperature and duration of chromite precipitation from the apatite. However, if the heating event lasted for a long time at high temperature, relatively coarse discrete chromite grains due to Ostwald ripening, rather than tiny grains, would be expected to occur, especially along the grain boundaries between apatite and the surrounding silicate phases. Considering that a heating event occurred responsible for the apatite replacement by merrillite and sulfidization of olivine, the exsolution of chromite in apatite could be another product of the transient heating event on the brachinite parent body.

Relict origin of apatite inclusions within silicate and chromite

Apatite is observed as inclusions within silicate and chromite from all three brachinites in this study. They either occur as individual grains or are associated with pore-free merrillite grains. Some merrillite grains occur as subhedral-euhedral grains included in the apatite inclusions. The apatite inclusions are distinctly different from those of the intergranular apatite and have two aspects of significance. First, most, if not all, of the apatite inclusions were probably protected by host chromite and silicate minerals and escaped replacement by merrillite. Second, most of the merrillite grains should have formed simultaneously with their host apatite grains rather than be a replacement product of the latter.

Apatite inclusions have been reported in a few brachinites (Brachina, Nehru et al. 1983) and brachinite-like achondrites (MIL 090340, Goodrich et al. 2017). However, the origin of the apatite inclusions was not discussed. Day et al. (2019) argued that the formation of phosphate inclusions within olivine in brachinites and brachinite-like achondrites could be related to the re-fertilization effect of a late-stage melt. However, the re-fertilization scenario cannot account for the textural and compositional features of the apatite and olivine inclusions within chromite in NWA 4969. First, chromite is a highly refractory mineral during partial melting (Arai 1994). It is unlikely that a chromite grain of residual origin includes phases that crystallize from late-stage re-fertilization melts. Second, the apatite inclusions within chromite from NWA 4969 are more F-rich than the intergranular apatite in the same sample. This observation contrasts with the expectation from the re-fertilization scenario that both the intergranular apatite and apatite inclusions would have similar chemical compositions. Third, if the olivine inclusion within chromite is genetically the same as the apatite inclusion within chromite, its higher Mg# also contrasts with the expected behavior that the equigranular olivine and the olivine inclusion would have similar compositions.

The above discussion suggests that apatite inclusions within chromite from brachinites (at least NWA 4969) cannot be a product of late-stage melt re-fertilization. Instead, the apatite inclusion (and associated merrillite), along with the intergranular apatite, probably formed under different processes, and the former should have formed earlier than the latter. One may propose a possibility that apatite and olivine inclusions in brachinites have a magmatic origin and are the earliest crystallizing phases from a mafic or ultramafic melt, given that some brachinites have been suggested to be cumulates (e.g., Warren and Kallemeyn 1989; Mittlefehldt et al. 2003). The observation that the olivine inclusions within chromite from NWA 4969 are more magnesian than the intergranular olivine seems to be consistent with this possibility. However, this scenario does not explain the early crystallization of apatite inclusions within chromite and their associated merrillite because Ca-phosphate minerals are typically late-stage crystallization phases in basaltic melts (Watson 1980). Therefore, the phosphate inclusions within chromite from the brachinites are not magmatic in origin, although we cannot exclude the possibility that the host brachinites might be cumulate in origin.

We propose that the apatite inclusions in brachinites could be relicts from the precursor materials of brachinites, while the intergranular apatite grains could be attributed to late-stage melt re-fertilization, following the idea that most brachinites are partial melt residues (e.g., Day et al. 2019, and references therein). A relict origin for the apatite inclusion can readily account for the presence of rare fluorapatite in NWA 4969, given that most intergranular apatite grains in brachinites are chlorapatite. If apatite crystallizes from a common Cl-rich, F-bearing melt, then no fluorapatite grains would be expected to occur, given that the other minerals are chemically homogeneous. This is contrary to observation. Similarly, such a scenario can also explain why intergranular apatite grains are not present in NWA 10637, but apatite inclusions are relatively common. We suspect that the apatite inclusions and associated phases within the chromite and olivine may have been prevented from partial melting or isolated from melts due to the protection of refractory chromite or silicate minerals, although Ca-phosphate minerals are less refractory than chromite and olivine (Watson 1980). However, based on the current observations, it is difficult to constrain the properties of potential precursor(s).

Comparison of apatite between brachinites and other meteorites

McCubbin and Jones (2015) and Ward et al. (2017) have compared the halogen compositions of apatite in different extraterrestrial materials. Apatite halogen compositions can be divided into three broad groups: (1) Apatite from ordinary chondrites, carbonaceous chondrites, and the achondrites GRA 06128/9 is mainly chlorapatite, although some apatite grains in carbonaceous chondrites are halogen-poor hydroxyapatite (Piralla et al. 2021 and references therein). (2) Apatite in martian meteorites

has a large variation in composition, almost covering the whole space in the Cl-F-OH ternary (McCubbin and Jones 2015; McCubbin et al. 2016). (3) Apatite from other achondrites (eucrites, winonaites, and acapulcoites) and lunar samples (Apollo samples and lunar meteorites) is mainly fluorapatite. Lastly, some apatite grains from ureilitic trachyandesite ALM-A contain equal amounts of chlorapatite and fluorapatite components (Ward et al. 2017). Ward et al. (2017) also studied the trace element compositions of Ca-phosphate minerals in different meteorites and found a large variation in the REE, U, and Th compositions among different groups of meteorites.

GRA 06128/9 are a pair of plagioclase-dominant achondrites that were suggested to be genetically associated with brachinites (Shearer et al. 2008, 2010; Day et al. 2009, 2012). Apatite is also an important accessory mineral in these meteorites (Day et al. 2009, 2012; Shearer et al. 2010, 2011; McCubbin and Jones 2015; Zhou et al. 2018). Apatite from GRA 06128/9 and brachinites are similar in two ways. First, both the apatite in GRA 06128/9 and the intergranular apatite in brachinites are chlorapatite, although the intergranular apatite in brachinites displays a much larger variation in the halogen composition and a higher OH/other anion component than those in GRA 06128/9 (Fig. 8a). Second, apatite from GRA 06128/9 has REE patterns and concentrations comparable to those of intergranular apatite in brachinites, although LREE in GRA 06128/9 apatite are relatively enriched compared to HREE (Fig. 9). However, there are two major differences for apatite and associated merrillite between GRA 06128/9 and brachinites. First, the apatite-merrillite texture in GRA 06128/9 distinctly differs from that of the intergranular apatite and merrillite in the brachinites. In GRA 06128/9, chlorapatite replaced or intergrew with merrillite (Shearer et al. 2011; Day et al. 2012; Zhou et al. 2018). In contrast, in the brachinites, intergranular chlorapatite was replaced by merrillite (this study). This distinction indicates different or even opposite halogen behaviors between GRA 06128/9 and the brachinites. Second, merrillite and apatite in GRA 06128/9 have different REE patterns (including different Eu anomalies). The REE concentrations in merrillite are higher by one order of magnitude than those in apatite (Shearer et al. 2010; Fig. 9). However, intergranular merrillite in brachinites has a REE pattern similar to that of the intergranular apatite (Fig. 9).

Based on the studies of McCubbin and Jones (2015) and Ward et al. (2017), apatite in chondrites has halogen compositions that are different from those in most achondrites (winonaites, acapulcoites, eucrites) and lunar samples. Interestingly, the Cl-rich feature of apatite in brachinites and GRA 06128/9 is similar to that in chondrites (Cl-rich) rather than other achondrites (F-rich), even primitive achondrites (winonaites and acapulcoites). Furthermore, the low concentrations of U and Th and the small positive Eu anomaly also resemble that found in apatite from chondrites (especially less-metamorphosed chondrites) rather than achondrites (Figs. 9 and 10; Zhang et al. 2016; Ward et al. 2017; Zhou et al. 2018). If all achondrites have a chondritic parent body, these similarities for apatite imply that brachinites probably retained the chemical features of their chondritic precursors more completely than other achondrites (e.g., eucrites, winonaites, and acapulcoites) and lunar samples. From this point of view, brachinites are a unique material that probably witnessed the earliest stage evolution of the achondrite parent body.

Implications

In the present study, two types of apatite in brachinites were observed: intergranular apatite and apatite inclusion within other minerals. Here intergranular chlorapatite in brachinites was replaced by merrillite, indicating halogen devolatilization on the brachinite parent body. This type of halogen devolatilization behavior has not been reported in the literature yet and differs from many previous investigations that proposed the replacement of merrillite by Cl-rich fluids on the asteroids and Mars. If an impact event was responsible for the devolatilization of halogen in brachinites, similar behavior probably takes place on other asteroids, the Moon, and even terrestrial planets, since the impact is one of the fundamental processes during planetary evolution.

Mn-Cr isotope systematics are very useful for the geo-chronology of the early solar system (Birck and Allègre 1988; Krot et al. 2006). However, one of the prerequisites of applying this chronological method is that the Mn-Cr system should be closed. Otherwise, the Mn-Cr age may be related to post-formation heating events or else be meaningless. Here fine chromite grains exsolved from apatite, indicating that Cr was probably locally or totally re-equilibrated among the different minerals during the heating event. If this is the case, the Cr isotopic compositions of different minerals in the brachinites are expected to have been disturbed or reset. For example, Dunlap et al. (2016a) obtained a young Mn-Cr age (4550.2 ± 0.8 Ma) for NWA 4882, which suggested a protracted thermal history (most likely from impact heating) on the brachinite parent body.

The large variation in halogen composition in an apatite aggregate (~40 μm) included in chromite from NWA 4969 (including the presence of fluorapatite) is a striking feature in this study. Such a large compositional variation has not been reported in metamorphic and igneous apatite from chondrites, eucrites, and primitive achondrites, although some apatite grains in ordinary chondrites, affected by impact-induced melting, exhibit a large variation in F and Cl abundances (Jones et al. 2016; Li and Hsu 2018; Wu and Hsu 2019). This implies that the halogen evolution of the brachinite parent body should be very complex and largely different from other primitive achondrites.

Acknowledgments and Funding

We thank Rhian H. Jones and an anonymous reviewer for their constructive and helpful comments, and Daniel Harlov for his editorial effort. This study was financially supported by National Natural Science Foundation of China (42025302, 41973061), the B-type Strategic Priority Program of the Chinese Academy of Sciences (XDB41000000), and the pre-research Project on Civil Aerospace Technologies funded by CNSA (D020204).

References cited

Adolfsson, E. and Hermansson, L. (2000) Phase stability aspects of various apatite-aluminum oxide composites. Journal of Materials Science, 35, 5719–5723, https://doi.org/10.1023/A:1004814726021.

Altree-Williams, A., Pring, A., Ngothai, Y., and Brügger, J. (2015) Textural and compositional complexities resulting from coupled dissolution–reprecipitation reactions in geomaterials. Earth-Science Reviews, 150, 628–651, https://doi.org/10.1016/j.earscirev.2015.08.013.

Arai, S. (1994) Characterization of spinel peridotites by olivine-spinel compositional relationships: Review and interpretation. Chemical Geology, 113, 191–204, https://doi.org/10.1016/0009-2541(94)90066-3.

Barrat, J.A., Zanda, B., Moynier, F., Bollinger, C., Liorzou, C., and Bayon, G. (2012) Geochemistry of CI chondrites: Major and trace elements, and Cu and Zn isotopes. Geochimica et Cosmochimica Acta, 83, 79–92, https://doi.org/10.1016/j.gca.2011.12.011.

Beard, S.P., Swindle, T.D., and Isachsen, C. (2016) Ar-Ar ages of brachinite and

brachinite-like achondrites. 79th Annual Meeting of the Meteoritical Society. Abstract 6411.

Birck, J.-L. and Allègre, C.J. (1988) Manganese-chromium isotope systematics and the development of the early solar system. Nature, 331, 579–584, https://doi.org/10.1038/331579a0.

Bouvier, A., Gattacceca, J., Grossman, J., and Metzler, K. (2017) The Meteoritical Bulletin, No. 105. Meteoritics & Planetary Science, 52, 2211, https://doi.org/10.1111/maps.12944.

Brearley, A.J. and Jones, R.H. (2018) Halogens in chondritic meteorites. In D.E. Harlov and L. Aranovich, Eds., The Role of halogens in terrestrial and extraterrestrial geochemical processes, 871–958. Springer Geochemistry.

Brey, G.P. and Köhler, T. (1990) Geothermobarometry in four-phase lherzo-lites II: New thermobarometers, and practical assessment of existing thermobarometers. Journal of Petrology, 31, 1353–1378, https://doi.org/10.1093/petrology/31.6.1353.

Collinet, M. and Grove, T.L. (2020) Widespread production of silica- and alkali-rich melts at the onset of planetesimal melting. Geochimica et Cosmochimica Acta, 277, 334–357, https://doi.org/10.1016/j.gca.2020.03.005.

Colson, R.O. (1992) Mineralization on the Moon? Theoretical considerations of Apollo 16 "rusty rocks", replacement in 67016, and surface-correlated volatiles on lunar volcanic glass. Proceedings 22nd Lunar and Planetary Science Conference, 427–436.

Connolly, H.C., Smith, C., Benedix, G., Folco, L., Righter, K., Zipfel, J., Yamaguchi, A., and Aoudjehane, H.C. (2008) The Meteoritical Bulletin, No. 93, 2008 March. Meteoritics & Planetary Science, 43, 571–632, https://doi.org/10.1111/j.1945-5100.2008.tb00673.x.

Crossley, S.D., Ash, R.D., Sunshine, J.M., Corrigan, C.M., McCoy, T.J., Mittlefehldt, D.W., and Puchtel, I.S. (2020) Sulfide-dominated partial melting pathways in brachinites. Meteoritics & Planetary Science, 55, 2021–2043, https://doi.org/10.1111/maps.13558.

Day, J.M.D., Ash, R.D., Liu, Y., Bellucci, J.J., Rumble, D. III, McDonough, W.F., Walker, R.J., and Taylor, L.A. (2009) Early formation of evolved asteroidal crust. Nature, 457, 179–182, https://doi.org/10.1038/nature07651.

Day, J.M.D., Walker, R.J., Ash, R.D., Liu, Y., Rumble, D. III, Irving, A.J., Goodrich, C.A., Tait, K., McDonough, W.F., and Taylor, L.A. (2012) Origin of felsic achondrites Graves Nunataks 06128 and 06129, and ultramafic brachinites and brachinite-like achondrites by partial melting of volatile-rich primitive parent bodies. Geochimica et Cosmochimica Acta, 81, 94–128, https://doi.org/10.1016/j.gca.2011.12.017.

Day, J.M.D., Corder, C.A., Rumble, D. III, Assayag, N., Cartigny, P., and Taylor, L.A. (2015) Differentiation processes in FeO-rich asteroids revealed by the achondrite Lewis Cliff 88763. Meteoritics & Planetary Science, 50, 1750–1766, https://doi.org/10.1111/maps.12509.

Day, J.M.D., Corder, C.A., Assayag, N., and Cartigny, P. (2019) Ferrous oxide-rich asteroid achondrites. Geochimica et Cosmochimica Acta, 266, 544–567, https://doi.org/10.1016/j.gca.2019.04.005.

Demnati, I., Grossin, D., Combes, C., Parco, M., Braceras, I., and Rey, C. (2012) A comparative physico-chemical study of chlorapatite and hydroxyapatite: From powders to plasma sprayed thin coatings. Biomedical Materials, 7, 054101, https://doi.org/10.1088/1748-6041/7/5/054101.

Dunlap, D.R., Romaniello, S.J., and Wadhwa, M. (2016a) ^{53}Mn-^{53}Cr systematics of the brachinite NWA 4882. 79th Annual Meeting of the Meteoritical Society. Abstract 6217.

Dunlap, D.R., Wadhwa, M., and Romaniello, S.J. (2016b) ^{53}Mn-^{53}Cr systematics of brachina revised in high precision. 47th Lunar and Planetary Science Conference. Abstract 3055.

Gardner-Vandy, K.G., Lauretta, D.S., and McCoy, T.J. (2013) A petrologic, thermodynamic and experimental study of brachinites: Partial melt residues of an R chondrite-like precursor. Geochimica et Cosmochimica Acta, 122, 36–57, https://doi.org/10.1016/j.gca.2013.07.035.

Gattacceca, J., McCubbin, F.M., Bouvier, A., and Grossman, J. (2020) Meteoritical Bulletin, No. 107. Meteoritics & Planetary Science, 55, 460–462, https://doi.org/10.1111/maps.13440.

Goodrich, C.A., Wlotzka, F., Ross, D.K., and Bartoschewitz, R. (2006) Northwest Africa 1500: Plagioclase-bearing monomict ureilite or ungrouped achondrite? Meteoritics & Planetary Science, 41, 925–952, https://doi.org/10.1111/j.1945-5100.2006.tb00496.x.

Goodrich, C.A., Kita, N.T., Spicuzza, M.J., Valley, J.W., Zipfel, J., Mikouchi, T., and Miyamoto, M. (2010) The Northwest Africa 1500 meteorite: Not a ureilite, maybe a brachinite. Meteoritics & Planetary Science, 45, 1906–1928, https://doi.org/10.1111/j.1945-5100.2010.01130.x.

Goodrich, C.A., Kita, N.T., Sutton, S.R., Wirick, S., and Gross, J. (2017) The Miller Range 090340 and 090206 meteorites: Identification of new brachinite-like achondrites with implications for the diversity and petrogenesis of the brachinite clan. Meteoritics & Planetary Science, 52, 949–978, https://doi.org/10.1111/maps.12846.

Grossman, J.N. and Brearley, A.J. (2005) The onset of metamorphism in ordinary and carbonaceous chondrites. Meteoritics & Planetary Science, 40, 87–122, https://doi.org/10.1111/j.1945-5100.2005.tb00366.x.

Harlov, D.E. (2015) Apatite: A fingerprint for metasomatic processes. Elements, 11, 171–176, https://doi.org/10.2113/gselements.11.3.171.

Henderson, C.E. (2011) Beam sensitive in EPMA: The analysis of apatite, $Ca_5(PO_4)_3(F,Cl,OH)$. Microscopy and Microanalysis, 17, 588–589, https://doi.org/10.1017/S1431927611003813.

Howarth, G.H., Pernet-Fisher, J.F., Bodnar, R.J., and Taylor, L.A. (2015) Evidence for the exsolution of Cl-rich fluids in Martian magmas: Apatite petrogenesis in the enriched lherzolitic shergottite Northwest Africa 7755. Geochimica et Cosmochimica Acta, 166, 234–248, https://doi.org/10.1016/j.gca.2015.06.031.

Hu, S., Lin, Y., Zhang, J., Hao, J., Xing, W., Zhang, T., Yang, W., and Changela, H. (2019) Ancient geologic events on Mars revealed by zircons and apatites from the Martian regolith breccia NWA 7034. Meteoritics & Planetary Science, 54, 850–879, https://doi.org/10.1111/maps.13256.

Hughes, J.M. and Rakovan, J.F. (2015) Structurally robust, chemically diverse: Apatite and apatite supergroup minerals. Elements, 11, 165–170, https://doi.org/10.2113/gselements.11.3.165.

Hughes, J.M., Jolliff, B.L., and Rakovan, J.F. (2008) The crystal chemistry of whitlockite and merrillite and the dehydrogenation of whitlockite to merrillite. American Mineralogist, 93, 1300–1305, https://doi.org/10.2138/am.2008.2683.

Hyde, B.C., Day, J.M.D., Tait, K.T., Ash, R.D., Holdsworth, D.W., and Moser, D.E. (2014) Characterization of weathering and heterogeneous mineral phase distribution in brachinite Northwest Africa 4872. Meteoritics & Planetary Science, 49, 1141–1156, https://doi.org/10.1111/maps.12320.

Ito, K., Niki, S., Hirata, T., Iizuka, T., and Mikouchi, T. (2022) U-Pb dating of phosphates in the brachinite meteorite Northwest Africa 10932. 53rd Lunar and Planetary Science Conference. Abstract 1744.

Jang, H.L., Lee, H.K., Jin, K., Ahn, H.Y., Lee, H.E., and Nam, K.T. (2015) Phase transformation from hydroxyapatite to the secondary bone mineral, whitlockite. Journal of Materials Chemistry B, Materials for Biology and Medicine, 3, 1342–1349, https://doi.org/10.1039/C4TB01793E.

Jolliff, B.L., Hughes, J.M., Freeman, J.J., and Zeigler, R.A. (2006) Crystal chemistry of lunar merrillite and comparison to other meteoritic and planetary suites of whitlockite and merrillite. American Mineralogist, 91, 1583–1595, https://doi.org/10.2138/am.2006.2185.

Jones, R.H., McCubbin, F.M., Dreeland, L., Guan, Y., Burger, P.V., and Shearer, C.K. (2014) Phosphate minerals in LL chondrites: A record of the action of fluids during metamorphism on ordinary chondrite parent bodies. Geochimica et Cosmochimica Acta, 132, 120–140, https://doi.org/10.1016/j.gca.2014.01.027.

Jones, R.H., McCubbin, F.M., and Guan, Y.B. (2016) Phosphate minerals in the H group of ordinary chondrites, and fluid activity recorded by apatite heterogeneity in the Zag H3–6 regolith breccia. American Mineralogist, 101, 2452–2467, https://doi.org/10.2138/am-2016-5728.

Keil, K. (2014) Brachinite meteorites: Partial melt residues from an FeO-rich asteroid. Chemie der Erde, 74, 311–329, https://doi.org/10.1016/j.chemer.2014.02.001.

Krot, A.N., Hutcheon, I.D., Brearley, A.J., Pravdivtseva, O.V., Petaev, M.I., and Hohenberg, C.M. (2006) Timescales and settings for alteration of chondritic meteorites. In D.S. Lauretta and H.Y. McSween Jr., Eds., Meteorites and the early Solar System II, 525–553. The University of Arizona Press.

Krot, A.N., Keil, K., Scott, E.R.D., Goodrich, C.A., and Weisberg, M.K. (2014) Classification of meteorites and their genetic relationships. In A.M. Davis, Ed., Treatise on Geochemistry, Vol. 2, Meteorites and Cosmochemical Processes, Elsevier, 1–63, https://doi.org/10.1016/B978-0-08-095975-7.00102-9.

Kullerud, G. and Yoder, H.S. Jr. (1963) Sulfide-silicate reactions, 215–218. Carnegie Institute of Washington Yearbook.

Li, Y. and Hsu, W. (2018) Multiple impact events on the L-chondritic parent body: Insights from SIMS U-Pb dating of Ca-phosphates in the NWA 7251 L-melt breccia. Meteoritics & Planetary Science, 53, 1081–1095, https://doi.org/10.1111/maps.13061.

Li, S., Hsu, W., Nemchin, A., Che, X., Liu, D., Long, T., Luo, Y., Beard, S., and Tang, C. (2021) Multiple thermal events recorded in IIE silicate inclusions: Evidence from in situ U-Pb dating of phosphates in Weekeroo Station. Geochimica et Cosmochimica Acta, 309, 79–95, https://doi.org/10.1016/j.gca.2021.06.017.

Liu, Y.S., Hu, Z.C., Gao, S., Günther, D., Xu, J., Gao, C.G., and Chen, H.H. (2008) In situ analysis of major and trace elements of anhydrous minerals by LA-ICP-MS without applying an internal standard. Chemical Geology, 257, 34–43, https://doi.org/10.1016/j.chemgeo.2008.08.004.

Maunaye, M., Hamon, C., L'Haridon, P., and Laurent, Y. (1976) Composés á structure apatite. IV. Étude structural de l'oxynitrure $Sm_8Cr_2Si_6N_2O_{24}$. Bulletin de la Société Française de Minéralogie et de Cristallographie, 99, 203–205.

McCubbin, F.M. and Jones, R.H. (2015) Extraterrestrial apatite: Planetary geochemistry to astrobiology. Elements, 11, 183–188, https://doi.org/10.2113/gselements.11.3.183.

McCubbin, F.M., Vander Kaaden, K.E., Tartèse, R., Klima, R.L., Liu, Y., Mortimer, J., Barnes, J.J., Shearer, C.K., Treiman, A.H., Lawrence, D.J., and others. (2015) Magmatic volatiles (H, C, N, F, S, Cl) in the lunar mantle, crust, and regolith: Abundances, distributions, processes, and reservoirs. American Mineralogist, 100, 1668–1707, https://doi.org/10.2138/am-2015-4934CCBYNCND.

McCubbin, F.M., Boyce, J.W., Srinivasan, P., Santos, A.R., Elardo, S.M., Filiberto, J., Steele, A., and Shearer, C.K. (2016) Heterogeneous distribution of H_2O in the Martian interior: Implications for the abundance of H_2O in depleted and enriched mantle sources. Meteoritics & Planetary Science, 51, 2036–2060, https://doi.org/10.1111/maps.12639.

McCubbin, F.M., Lewis, J.A., Barnes, J.J., Elardo, S.M., and Boyce, J.W. (2021) The abundance of F, Cl, and H_2O in eucrites: Implications for the origin of volatile depletion in the asteroid 4 Vesta. Geochimica et Cosmochimica Acta, 314, 270–293,

https://doi.org/10.1016/j.gca.2021.08.021.
Mittlefehldt, D.W. (2014) Achondrites. In A.M. Davis, Ed., Treatise on Geochemistry, Vol. 2, Meteorites and Cosmochemical Processes, Elsevier, 235–266, https://doi.org/10.1016/B978-0-08-095975-7.00108-X.
Mittlefehldt, D.W., Bogard, D.D., Berkley, J.L., and Garrison, D.H. (2003) Brachinites: Igneous rocks from differentiated asteroid. Meteoritics & Planetary Science, 38, 1601–1625, https://doi.org/10.1111/j.1945-5100.2003.tb00004.x.
Nehru, C.E., Prinz, M., Delaney, J.S., Dreibus, G., Palme, H., Spettel, B., and Wänke, H. (1983) Brachina: A new type of meteorite, not a chassignite. Journal of Geophysical Research, 88(S01), B237–B244, https://doi.org/10.1029/JB088iS01p0B237.
Norman, M.D. and Nemchin, A.A. (2014) A 4.2 billion year old impact basin on the Moon: U-Pb dating of zirconolite and apatite in lunar melt rock 67955. Earth and Planetary Science Letters, 388, 387–398, https://doi.org/10.1016/j.epsl.2013.11.040.
Norman, M.D., Keil, K., Griffin, W.L., and Ryan, C.G. (1995) Fragments of ancient lunar crust: Petrology and geochemistry of ferroan noritic anorthosites from the Descartes region of the Moon. Geochimica et Cosmochimica Acta, 59, 831–847, https://doi.org/10.1016/0016-7037(94)00363-Q.
Pan, Y.M. and Fleet, M.E. (2002) Compositions of the apatite-group minerals: Substitution mechanisms and controlling factors. Reviews in Mineralogy and Geochemistry, 48, 13–49, https://doi.org/10.2138/rmg.2002.48.2.
Petaev, M.I., Barsukova, L.D., Lipschutz, M.E., Wang, M.S., Ariskin, A.A., Clayton, R.N., and Mayeda, T.K. (1994) The Divnoe meteorite: Petrology, chemistry, oxygen isotopes and origin. Meteoritics, 29, 182–199, https://doi.org/10.1111/j.1945-5100.1994.tb00671.x.
Piralla, M., Tartèse, R., Marrocchi, Y., and Joy, K.H. (2021) Apatite halogen and hydrogen isotope constraints on the conditions of hydrothermal alteration in carbonaceous chondrites. Meteoritics & Planetary Science, 56, 809–828, https://doi.org/10.1111/maps.13639.
Putnis, A. (2002) Mineral replacement reactions: From macroscopic observations to microscopic mechanisms. Mineralogical Magazine, 66, 689–708, https://doi.org/10.1180/0026461026650056.
——— (2009) Mineral replacement reactions. Reviews in Mineralogy and Geochemistry, 70, 87–124, https://doi.org/10.2138/rmg.2009.70.3.
Putnis, A. and John, T. (2010) Replacement processes in the Earth's crust. Elements, 6, 159–164, https://doi.org/10.2113/gselements.6.3.159.
Rumble, D., Irving, A.J., Bunch, T.E., Wittke, J.H., and Kuehner, S.M. (2008) Oxygen isotopic and petrological diversity among brachinites NWA 4872, NWA 4874, NWA 4882 and NWA 4969: How many ancient parent bodies? Lunar and Planetary Science XXXIX. Abstract 1974.
Sarafian, A.R., Roden, M.F., and Patiño-Douce, A.E. (2013) The volatile content of Vesta: Clues from apatite in eucrites. Meteoritics & Planetary Science, 48, 2135–2154, https://doi.org/10.1111/maps.12124.
Sharp, T.G. and DeCarli, P.S. (2006) Shock effects in meteorites. In D.S. Lauretta and H.Y. McSween Jr., Eds., Meteorites and the early Solar System II, 653–677. The University of Arizona Press.
Shearer, C.K., Burger, P.V., Neal, C.R., Sharp, Z.D., Borg, L.E., Spivak-Birndorf, L., Wadhwa, M., Papike, J.J., Karner, J.M., Gaffney, A.M., and others. (2008) A unique glimpse into asteroidal melting processes in the early solar system from the Graves Nunatak 06128/06129 achondrites. American Mineralogist, 93, 1937–1940, https://doi.org/10.2138/am.2008.3056.
Shearer, C.K., Burger, P.V., Neal, C.R., Sharp, Z.D., Spivak-Birndorf, L., Borg, L.E., Fernandes, V.A., Papike, J.J., Karner, J.M., Wadhwa, M., and others. (2010) Non-basaltic asteroidal magmatism during the earliest stages of solar system evolution. A view from Antarctic achondrites Graves Nunatak 06128 and 06129. Geochimica et Cosmochimica Acta, 74, 1172–1199, https://doi.org/10.1016/j.gca.2009.10.029.
Shearer, C.K., Burger, P.V., Papike, J.J., Sharp, Z.D., and McKeegan, K.D. (2011) Fluids on differentiated asteroids: Evidence from phosphates in differentiated meteorites GRA 06128 and GRA 06129. Meteoritics & Planetary Science, 46, 1345–1362, https://doi.org/10.1111/j.1945-5100.2011.01233.x.
Shearer, C.K., Burger, P.V., Guan, Y., Papike, J.J., Sutton, S.R., and Atudorei, N.V. (2012) Origin of sulfide replacement textures in lunar breccias. Implications for vapor element transport in the lunar crust. Geochimica et Cosmochimica Acta, 83, 138–158, https://doi.org/10.1016/j.gca.2011.11.031.
Shearer, C.K., Burger, P.V., Papike, J.J., McCubbin, F.M., and Bell, A.S. (2015) Crystal chemistry of merrillite from Martian meteorites: Mineralogical recorders of magmatic processes and planetary differentiation. Meteoritics & Planetary Science, 50, 649–673, https://doi.org/10.1111/maps.12355.
Singerling, S.A., McCoy, T.J., and Gardner-Vandy, K.G. (2013) Possible evidence for sulfidization reactions in the Miller Range brachinites(?). 44th Lunar and Planetary Science Conference. Abstract 1669.
Swindle, T.D., Kring, D.A., Burkland, M.K., Hill, D.H., and Boynton, W.V. (1998) Noble gases, bulk chemistry, and petrography of olivine-rich achondrites Eagles Nest and Lewis Cliff 88763: Comparison to brachinites. Meteoritics & Planetary Science, 33, 31–48, https://doi.org/10.1111/j.1945-5100.1998.tb01605.x.
Wadhwa, M., Shukolyukov, A., and Lugmair, W. (1998) ^{53}Mn-^{53}Cr systematics in Brachina: a record of one of the earliest phases of igneous activity on an asteroid. Lunar and Planetary Science XXIX. Abstract 1480.
Wang, S.Z., Zhang, A.C., Pang, R.L., Li, Y., and Chen, J.N. (2019) Possible records of space weathering on Vesta: Case study in a brecciated eucrite Northwest Africa 1109. Meteoritics & Planetary Science, 54, 836–849, https://doi.org/10.1111/maps.13254.
Ward, D., Bischoff, A., Roszjar, J., Berndt, J., and Whitehouse, M.J. (2017) Trace element inventory of meteoritic Ca-phosphates. American Mineralogist, 102, 1856–1880, https://doi.org/10.2138/am-2017-6056.
Warren, P.H. and Kallemeyn, G.W. (1989) Allan Hills 84025: The second brachinite, far more differentiated than Brachina, and an ultramafic achondritic clast from L chondrite Yamato 75097. Proceedings of 19th Lunar and Planetary Science Conference, 475–486.
Watson, E.B. (1980) Apatite and phosphorus in mantle source regions: An experimental study of apatite/melt equilibria at pressures at 25 kbar. Earth and Planetary Science Letters, 51, 322–335, https://doi.org/10.1016/0012-821X(80)90214-9.
Wu, Y. and Hsu, W. (2019) Petrogenesis and in situ U-Pb geochronology of a strongly shocked L-melt rock Northwest Africa 11042. Journal of Geophysical Research. Planets, 124, 893–909, https://doi.org/10.1029/2018JE005743.
Yin, Q.Z., Zhou, Q., Li, Q.L., Li, X.H., Liu, Y., Tang, G.Q., Krot, A.N., and Jenniskens, P. (2014) Records of the Moon-forming impact and the 470 Ma disruption of the L chondrite parent body in the asteroid belt from U-Pb apatite ages of Novato. Meteoritics & Planetary Science, 49, 1426–1439, https://doi.org/10.1111/maps.12340.
Zhang, A.C., Hsu, W.B., Floss, C., Li, X.H., Li, Q.L., Liu, Y., and Taylor, L.A. (2010) Petrogenesis of lunar meteorite Northwest Africa 2977: Constraints from in situ microprobe results. Meteoritics & Planetary Science, 45, 1929–1947, https://doi.org/10.1111/j.1945-5100.2010.01131.x.
Zhang, A.C., Wang, R.C., Hsu, W.B., and Bartoschewitz, R. (2013) Record of S-rich vapors on asteroid 4 Vesta: Sulfurization in the Northwest Africa 2339 eucrite. Geochimica et Cosmochimica Acta, 109, 1–13, https://doi.org/10.1016/j.gca.2013.01.036.
Zhang, A.C., Li, Q.L., Yurimoto, H., Sakamoto, N., Li, X.H., Hu, S., Lin, Y.T., and Wang, R.C. (2016) Young asteroidal fluid activity revealed by absolute age from apatite in carbonaceous chondrite. Nature Communications, 7, 12844, https://doi.org/10.1038/ncomms12844.
Zhang, A.C., Bu, Y.F., Pang, R.L., Sakamoto, N., Yurimoto, H., Chen, L.H., Gao, J.F., Du, D.H., Wang, X.L., and Wang, R.C. (2018) Origin and implications of troilite-orthopyroxene intergrowths in the brecciated diogenite Northwest Africa 7183. Geochimica et Cosmochimica Acta, 220, 125–145, https://doi.org/10.1016/j.gca.2017.09.051.
Zhang, A.C., Kawasaki, N., Bao, H., Liu, J., Qin, L., Kuroda, M., Gao, J.F., Chen, L.H., He, Y., Sakamoto, N., and others. (2020) Evidence of metasomatism in the interior of Vesta. Nature Communications, 11, 1289, https://doi.org/10.1038/s41467-020-15049-7.
Zhang, L., Zhang, A.C., and Wang, S.Z. (2021a) Thermal evolution of brachinite meteorites. The First National Planetary Conference. Suzhou, China, June 18–22, 2021.
——— (2021b) Mineralogical records of thermal evolution on the brachinite parent body. The Seventh Youth Geoscience Forum, Guiyang, China, July 9–11, 2021.
Zhou, Q., Yin, Q.Z., Shearer, C.K., Li, X.H., Li, Q.L., Liu, Y., Tang, G.Q., and Li, C.L. (2018) U-Pb and Pb-Pb apatite ages for Antarctic achondrite Graves Nunataks 06129. Meteoritics & Planetary Science, 53, 448–466, https://doi.org/10.1111/maps.13026.

Manuscript received July 17, 2022
Manuscript accepted October 13, 2022
Accepted manuscript online October 27, 2022
Manuscript handled by Daniel E. Harlov

Endnote:

[1]Deposit item AM-23-98712. Online Materials are free to all readers. Go online, via the table of contents or article view, and find the tab or link for supplemental materials.